Silicon single photon imaging detectors*

D. F. Figer[†a], B. F. Aull[b], D. R. Schuette[b], B. J. Hanold[a], K. Kolb[a], J. Lee[a]
[a]Center for Detectors, Rochester Institute of Technology,
74 Lomb Memorial Drive, Rochester, NY 14623;
[b]Lincoln Laboratory, Massachusetts Institute of Technology,
244 Wood St, Lexington, MA 02420

ABSTRACT

Single-photon imaging detectors promise the ultimate in sensitivity by eliminating read noise. These devices could provide extraordinary benefits for photon-starved applications, *e.g.*, imaging exoplanets, fast wavefront sensing, and probing the human body through transluminescence. Recent implementations are often in the form of sparse arrays that have less-than-unity fill factor. For imaging, fill factor is typically enhanced by using microlenses, at the expense of photometric and spatial information loss near the edges and corners of the pixels. Other challenges include afterpulsing and the potential for photon self-retriggering. Both effects produce spurious signal that can degrade the signal-to-noise ratio. This paper reviews development and potential application of single-photon-counting detectors, including highlights of initiatives in the Center for Detectors at the Rochester Institute of Technology and MIT Lincoln Laboratory. Current projects include single-photon-counting imaging detectors for the Thirty Meter Telescope, a future NASA terrestrial exoplanet mission, and imaging LIDAR detectors for planetary and Earth science space missions.

Keywords: detector, read noise, avalanche photodiode, array

INTRODUCTION

Single-photon detectors (SPDs) have the desirable property of detecting signal without adding electrical noise in the readout process. By digitizing the signal at the earliest stage of the detection process, these devices effectively remove many common noise sources. Detector read noise is an important contributor to system noise in low-flux applications, *e.g.*, faint object imaging or bright source imaging in cases where the photon flux is dispersed in time, space, or energy. Building larger telescopes and more complex instruments can improve sensitivity for photon starved applications, but at extreme costs for the largest and most sophisticated systems. An alternative is to use "noiseless" detectors that count each incoming photon. These types of detectors would improve sensitivity while dramatically reducing system complexity and the consumption of resources, *e.g.*, size, weight, and power.

In support of this approach, note Equation 1 which expresses the exposure time required for a system to yield a signal-to-noise ratio of one, in the limit of negligible background flux and detector dark current. In this case, the read noise (N_{read}) is just as important as quantum efficiency (QE) and optical aperture area (embedded in the collected source flux, N_γ).

$$\tau \xrightarrow{SNR=1 \text{ and } N_{\gamma,background}=0 \text{ and } i_{dark}=0} \frac{N_{read}\sqrt{n_{pix}}}{N_\gamma QE}. \qquad \text{Equation 1}$$

APPLICATIONS

SPDs may be effective in applications spanning astronomy, biophotonics, remote sensing, quantum optics, communications, encryption, and military. The following highlights two applications.

---

* The MIT Lincoln Laboratory portion of this work was performed under a Collaboration Agreement between MIT Lincoln Laboratory and Rochester Institute of Technology. Opinions, interpretations, conclusions, and recommendations are those of the authors, and do not necessarily represent the view of the United States Government.

† figer@cfd.rit.edu; phone 1 585 475-6005; fax 1 585 475-4250; http://ridl.cfd.rit.edu

Astronomical imaging

We can consider a typical test case to dramatize the benefit of a photon-counting detector for astronomical imaging. Figure 1 (*left*) contains a table of exposure times needed to achieve SNR=1 per spectral element[‡] as a function of read noise and quantum efficiency for a 30th magnitude planet imaged in a low-resolution spectrograph with background contributions from zodiacal light and spillover from a nearby star, suppressed by 10^{10} using realizable nulling techniques [1]. The dark current is 0.001 electrons/second/pixel. We assume that R=100, where R is defined as the wavelength divided by the wavelength of a resolution element. The table shows that the observing time would be about a ***factor of two less*** with a photon-counting detector compared to a typical CCD. Figure 1 (*right*) is a graphic representation of the data in the table for QE=70%. While this spectroscopic case is most dramatic, the planet imaging detector and wavefront sensor would also benefit from photon-counting technology.

Exposure Time (seconds) for SNR = 1				
FOM		Quantum Efficiency		
		50%	70%	100%
read noise	0	680	453	300
	1	865	591	400
	2	1,209	841	577
	3	1,587	1,113	768
	4	1,976	1,392	964
	5	2,369	1,673	1,161
	6	2,764	1,956	1,359
	7	3,161	2,239	1,558
mag_star=5, mag_planet=30, R=100, i_dark=0.0010				

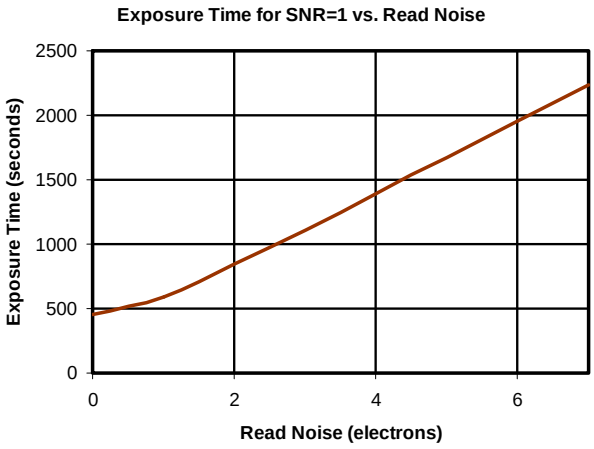

Figure 1. (left) A photon-counting detector (zero read noise) would deliver dramatic gains versus typical CCDs in system sensitivity and thus time to detect a planet. The table shows the time needed to reach SNR=1 versus read noise and quantum efficiency for a 30th magnitude planet imaged in a spectrograph (R=100) with background contributions from zodiacal light and spillover from a nearby star light, suppresed by 10^{10}. System parameters are from TPF-C Flight Baseline Mission Concept Report [2] and the TPF-C STDT Report [3]. The dark current is 0.001 e^-/second/pixel. (right) This is a plot of the data in the table for QE=70%.

Wavefront Sensing

Consider a typical test case that dramatizes the benefit of a single photon detector for wavefront sensing applications, in particular for correcting atmospheric-induced PSF motion by observing a sharpened tip-tilt star. Table 1 gives limiting magnitudes to achieve SNR=4 as a function of read noise and PDE with a 10-meter telescope, a frame rate of 3,000 Hz, and a waveband that includes 1.05-1.54 μm; we refer to this waveband as "JH2." The table demonstrates the dramatic value of a zero read noise detector. From the table, it appears that such a detector would offer three magnitudes greater sensitivity than existing infrared detectors. This assumes that one could operate existing detectors at such a high frame rate (doubtful) and that the read noise would be ~50 e^-. This noise figure is extrapolated from noise of existing infrared devices (~15 e^-) at 30 Hz frame rate, assuming that one scales from a pixel read frequency of 100 kHz for a 2048×2048 pixel H2RG with 32 outputs [4] to a 256×256-pixel device with 1 output and a pixel read frequency of 5 MHz. Approximately 2.3 stars per field yields 90% sky coverage at the North Galactic Pole [5]. This density corresponds to a JH2 magnitude of ~16.5 for a one square arcminute field. In fact, if one were to operate the device more slowly (500 frames/second), then it would deliver SNR=4 for JH2 magnitude ~18.0, dramatically increasing sky coverage and extending sensitivity even well into the range of Active Galactic Nuclei (AGN).

[‡] This level of signal quality is at the threshold to detect the presence of absorption bands of water, ozone, other molecules, vegetation, and oceans, which might be expected in spectra of terrestrial planets [17].

jh2-band Magnitude for SNR=4 and Frame Rate=3000 Hz											
FOM		Photon Detection Efficiency (PDE)									
		10%	20%	30%	40%	50%	60%	70%	80%	90%	100%
read noise (e^-)	0	14.7	15.5	15.9	16.2	16.4	16.6	16.8	16.9	17.1	17.2
	1	14.3	15.0	15.5	15.8	16.0	16.2	16.4	16.5	16.6	16.8
	2	13.8	14.6	15.0	15.3	15.6	15.8	15.9	16.1	16.2	16.3
	3	13.5	14.2	14.7	15.0	15.2	15.4	15.6	15.7	15.9	16.0
	4	13.2	14.0	14.4	14.7	15.0	15.2	15.3	15.5	15.6	15.7
	5	13.0	13.7	14.2	14.5	14.7	14.9	15.1	15.3	15.4	15.5
	10	12.3	13.1	13.5	13.8	14.1	14.3	14.4	14.6	14.7	14.8
	20	11.6	12.3	12.8	13.1	13.3	13.5	13.7	13.8	14.0	14.1
	50	10.6	11.4	11.8	12.1	12.4	12.6	12.7	12.9	13.0	13.1

Table 1. Limiting magnitude for a tip-tilt star in JH2 band, assuming 3000 Hz frame rate, a 10 meter telescope, and SNR=4, as a function of read noise and PDE. The PDE goal for the device is 40%, so the predicted magnitude limit is ~16.2. Assuming that existing devices could be operated at 3000 Hz, we would predict read noise of ~50 e^-, giving a JH2 limit of 12.9, or over three magnitudes brighter.

SINGLE PHOTON DETECTORS

Common SPD architectures use charge gain or sharp transitions in material electrical properties. In both cases, the devices amplify the signal to a level that is generally far greater than any system electrical noise.

Table 2 gives a sample of superconducting and semiconducting SPDs. The superconducting SPDs have the advantage that they can, in principle, measure photon energy. This paper focuses on semiconducting SPDs.

Table 2. Single Photon Detector Technologies.

Superconductors	Semiconductors
Transition Edge Sensor (TES) pro: energy resolution con: operating temperature of tens of mK	Electron Multiplying CCD (EMCCD) pro: commercially available con: excess noise factor
Superconducting Tunnel Junction (STJ) pro: energy resolution con: operatinfg temperature of mK, leakage current	Linear Mode Avalance Photodiode (LM-APD) pro: ns time constant con: excess noise factor (although HgCdTe has ~no excess noise)
Kinetic Inductance Detector (KID) pro: energy resolution con: ms time constant	Geiger Mode Avalance Photodiode (GM-APD) pro: large pulse per photon con: afterpulsing
Superconducting Single Photon Detectors (SSPD) pro: ns time constant con: low fill-factor, polarized, few K	

CCDs are the most mature electronic imaging detectors, and their performance is near-ideal in many important parameters. That is, they can have near-unity QE over the near-UV to one micron waveband, read noise of only a few electrons, and dark current that can typically be reduced to a negligible level by cooling. They are generally not effective for resolving energy, except for photon energies above a few tens of eV. In addition, they cannot detect photons having less than ~1 eV of energy, assuming that they are made of silicon.

Electron-multiplying CCDs (EMCCDs) can deliver photon-counting capability by applying high gain at the output of a conventional CCD. In this mode of operation, a single photon produces on order of a thousand electrons at the output. A

comparator generates an event signal if this packet exceeds the threshold. This approach is less advantageous as the flux contributes more than one electron of integrated charge per pixel per read time interval. In this case, the output voltage is still above the threshold, and the excess photons are "lost." These devices can potentially run at high frame rate without a read noise penalty, thus enabling "lucky imaging" in ground-based applications [6]. The GAIA mission considered EMCCDs, but chose another conventional CCDs [7].

These devices can be operated with a more sophisticated digitizing circuit on the output, so that the discrete jumps in the output charge can be recognized as corresponding to different numbers of absorbed photons. One compromise to this approach is that the effective shot noise is increased by a factor of square-root of two *higher* than even a conventional CCD because of uncertainty in the gain. Even in systems that typically experience low fluxes, it is still often desirable to accommodate higher flux levels. Therefore, it is important to use a detector that preserves the advantages of photon-counting at arbitrary flux levels. Having the electron multiplying stage at an output, instead of inside of each pixel, severely limits the length of the read time window because many pixels must be read through the same output before the device can be clocked through a new exposure. One way to ensure that only one event is counted at a time is to dramatically increase the read rate, but this increases clock induced charge (CIC). This effect contributes an effective dark current noise contribution to the output signal. In effect, then, the desire to limit events to single photons competes with the desire to minimize CIC. Even after mitigation effects (inverted clocks), CIC generates about 0.0015 e^-/pixel/read in spurious charge at −20 C. If the device is read at 10 Hz frame rate for a 1 minute exposure, that implies 600 reads, or 0.9 e^-/pixel, enough to generate a false event 90% of the time. While CIC can be reduced with additional cooling, it will still degrade SNR. In addition to these problems, the EMCCD suffers from charge bleeding below −100 °C [8], gain instability, CTE loss at low temperature, and typical radiation-induced CTE degradation with exposure to space radiation. The EMCCD is more susceptible to radiation damage than traditional CCDs [9], [10], [7]. This is due to radiation-induced bandgap states near the high field regions of the gain register elements. After exposure to 5 krad(Si) of high-energy protons, the sum of the induced dark current in the output and gain registers is 0.4 e^-/gain element/pixel for a nominal read rate of 11 MHz at −20 C (Mark Robbins, e2v, 2009, private communication). A Monte Carlo simulation predicts an average output charge of about 500 e^-/pixel from this contribution. Cooling will help reduce this effect, but it will always be present in an EMCCD.

One of the most promising technologies for delivering broad-band single photon counting detectors is represented by avalanche photodiodes that leverage standard CMOS foundry processing to implement a densely packed in-pixel circuit that controls a photodiode and counts photon events. These devices have already demonstrated single-photon detection capability in modest format sizes and can use detector arrays that are sensitive to x-ray through mid-infrared wavelengths.

In particular, several groups are developing LM-APD and GM-APD arrays in silicon, InGaAs, and HgCdTe, mated to silicon readout circuits that have in-pixel counting and time-tagging capability. It is likely that megapixel scale detectors will be ready for astrophysics applications in the five-year time scale, ripe for use in extremely large telescopes and planet finding space missions.

AVALANCHE PHOTODIODES

Avalanche photodiodes produce a large signal in response to photogenerated charge. Free electron-hole pairs in a semiconductor lattice tend to wander according to a random walk until they recombine. Along this path, they may interact with atoms in the lattice, causing phonon excitation, but not liberating more charge into the conduction band. In the presence of a strong enough electric field, however, the charge can attain enough kinetic energy to dislodge another electron-hole pair. These newly freed carriers immediately accelerate in the strong field and create more free electron-hole pairs, ultimately causing an avalanche of charge. Once this avalanche has begun, a competition develops between the creation and removal rate of free electron-hole pairs [11].

At biases below the breakdown voltage (V_{BR}), removal dominates, causing the avalanche current to decay and ultimately cease. The gain (M) is the number of carriers generated during an avalanche by a single initiating carrier. In the absence of a quenching phenomenon, M is finite and determined by the statistics of the avalanche process. This type of operation is called linear-mode, since photocurrent is proportional to incident photon flux.

For linear-mode operation, Equation 2 defines an empirical relationship between M and the reverse bias V_{app}. The material-dependent factor m is typically between three and six. At low applied voltage, M~1, and the current obeys the

classical ideal diode equation. As V_{app} approaches V_{BR}, M becomes large and the current is equal to the saturation current in the ideal diode equation times M [11].

$$M = \frac{1}{1 - \left[\frac{|V_{app}|}{V_{BR}}\right]^{m}} \qquad \text{Equation 2}$$

In the case where the bias is above V_{BR}, multiplication outpaces removal, and Equation 2 is no longer valid. Initially, the avalanche process causes exponential growth of the current. After some length of time, enough electrons and holes accumulate respectively at the n- and p-sides of the depletion region to create an internal electric field that opposes the applied bias and arrests the growth of the current. The device remains in conduction until the circuit reduces the applied bias (quenches the device), allowing the APD to turn off. In this type of operation, known as Geiger-mode, the gain would be infinite if the bias were held above breakdown. With quenching, however, the gain is determined by the circuit rather than by the avalanche statistics. In either case, an electrical event resulting from a single incident photon is indistinguishable from one initiated by a larger number of simultaneously arriving photons.

It is important to note that even in Geiger-mode operation, there is a probability that the avalanche may terminate in its earliest stages due to fluctuations and result in a non-detectable signal. While gain is an important metric for linear-mode operation, Geiger-mode operation is better characterized by the probability that the avalanche will become self-sustaining, referred to as the avalanche initiation probability.

Applications that utilize APDs take advantage of the avalanche mechanism to boost signal from a single incident photon. For example, an observation of a target emitting very low photon flux may have a low signal-to-noise ratio (SNR) if the photocurrent is similar in magnitude to the dark current or to the readout noise. Because of the structure of the APD, most of its dark current is generated at the periphery of the device and dose not get multiplied. Because an avalanche multiplies the signal without multiplying most of the dark current, the SNR greatly improves and the target becomes discernable in the observation [11].

GEIGER-MODE AVALANCHE PHOTODIODE

An avalanche photodiode operated in Geiger-mode produces a *digital* pulse *directly from the photodiode* in response to the absorption of a single photon, i.e. digitization is done in-pixel (see Figure 2). The operation of a GM-APD is conceptually simple. The APD is charged to a reverse bias voltage that *exceeds* the breakdown voltage by a few volts, and then is left in an open-circuit configuration. The absorption of a photon creates an electron-hole pair that is accelerated and multiplied in a chain of impact ionizations that creates secondary electrons and holes, just as in a traditional linear-mode APD operated below breakdown. As noted above, the electric fields in a device biased above breakdown are strong enough that the multiplication process outpaces the extraction of carriers, resulting initially in exponential growth of current. This current growth saturates after a few tens of picoseconds because of space charge effects and device resistance. Therefore, the APD switches from an "off" state to a state in which it is conducting current. It then discharges its own capacitance until its bias falls to below breakdown, at which point the avalanche is no longer self-sustaining and the APD turns off. With appropriate biasing of the APD, this discharge voltage pulse is level shifted to fall within a CMOS-logic-compatible range. Once the APD has had adequate time to turn off and release any trapped carriers, it can be reset for the next detection.

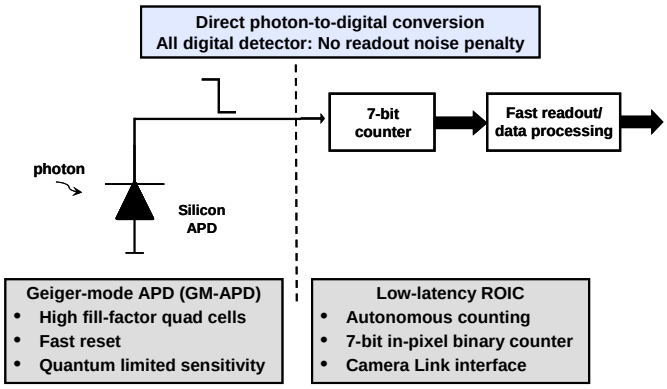

Figure 2. Schematic representation of an APD pixel. The photodiode circuit generates a digital pulse for each incoming photon. Events are accumulated by an in-pixel counter before being read out.

Detectors based on this principle digitize photon arrival times or rates within the pixel circuit; therefore, they have quantum-limited sensitivity and zero readout noise. While the GM-APDs need several tens of volts to be biased in the Geiger mode, only digital-like voltage transitions are required to operate the detector, thereby avoiding the power dissipation and mass associated with analog digitizing circuits. They are resilient to radiation for several reasons, but primarily because the signal charge is not clocked across charge traps in neighboring pixels, *e.g.*, as in a conventional CCD.

DEVICE CHARACTERISTICS

In general, systems based on APDs have a common set of characteristics that limit their performance. These include properties that are common to most detectors, like dark signal, and also some that are more peculiar to Geiger-mode APDs, *e.g.*, avalanche initiation probability. The following describes the most relevant characteristics of these devices.

Dead time

Dead time is the time during an exposure when the detector cannot accumulate signal. This effect can be due to the finite reset time of a circuit, or the inability of the circuit to distinguish between multiple absorbed photons within a short time period. For instance, in Geiger mode, an APD has the same response to a short light pulse, regardless of the number of photons in the pulse. In linear mode, an APD will generate more charge with each additional absorbed photon. In this case, the architecture of the sensing circuit determines whether the additional charge is counted as additional signal. Dead time reduces the effective exposure time and results in a loss of efficiency.

Avalanche initiation probability

The avalanche initiation probability is the probability that a large enough avalanche will be established such that the output voltage exceeds the event trigger threshold voltage in the sensing circuit. Failure to initiate a large enough avalanche represents a loss in total system efficiency. Avalanche chains are random processes, and for a given bias and location of the primary electron-hole pair, there is a finite probability that an avalanche will terminate prematurely due to fluctuations.

Dark events

These are events that are triggered by multiplied dark current. Most of the dark charge is generated at surfaces and does not initiate an avalanche. The dark charge that is multiplied and results in events is from the bulk. That component of dark current is dominated by thermal generation-recombination that decreases with decreasing temperature. Based on previous measurements of the GM-APDs, we expect dark count rates of several kHz at room temperature. Dark count rate is measured by operating the device in the dark and calculating the mean time of event generation.

Afterpulsing

Afterplusing describes the tendency of an individual APD pixel to produce a burst of events after an avalanche has been initiated and quenched in that pixel. An afterpulse can be triggered when charge produced in the original avalanche

becomes trapped in material defect sites and later migrates from the trap to the high field region. It can also be produced if charge generated by APD light emission is temporarily stored in the absorber region while the depletion region is debiased. Afterpulsing is a function of avalanche time, quench time, pixel geometry, field geometry, biasing, and the trap population. Afterpulsing can be measured by correlating event times. A device that generates a high level of afterpulsing will tend to show elevated dark count rates just after an event.

PREVIOUS WORK

The device design used for this project has evolved from a series of devices designed by Lincoln Laboratory [12], [13], [14], [15]. The sensitivity and noise-free readout of these devices provided significant benefits in system performance. In the original applications, accuracy in timing of individual photon events is the most important performance metric. Previous LIDAR demonstrations validated the utility of photon-counting detector array technology, in particular for tactical military applications [16].

Development of this technology at Lincoln Laboratory started in the mid 1990's, with initial interest focused on tactical military laser radar imaging. In 1997, the principle of "photon-to-digital" conversion was demonstrated by wire bonding a 4×4 APD array to a CMOS chip with 16 digital timing circuits. The simplicity of direct connection between detector and CMOS logic was an enabler for building 3D imaging systems. The arrays were scaled up to 32×32 format and techniques were developed to hybridize to CMOS readouts. By 2005, hybridized arrays with timing resolutions in the 250 ps range had been fabricated, packaged, and incorporated into airborne laser radar systems that demonstrated foliage penetration and rapid terrain mapping. The APDs developed for these systems are inherently low fill factor devices (5-7%), and light concentration was achieved either by using microlenses or by transmitting an array of light spots onto the scene.

Current efforts are focused on development of larger format (256×256) high fill factor APD arrays for passive imaging, as is needed for the current project. A novel CMOS readout architecture was developed that simultaneously provides a small pixel (25 μm), high dynamic range, and low readout bandwidth. Learning from experience with quad-cell arrays used for wavefront sensing, Lincoln Laboratory is developing new APD structures that will combine high detection efficiency (>70%) with low dark count rate (sub-kHz with modest TE cooling). Two new improvements for the current project are the use of a larger photon absorbing region and a bonded architecture that allows for backside illumination. These features combine to deliver high fill factor compared to previous LIDAR pixel designs which have relatively low fill factor. This is particularly important for imaging very faint point sources, where it is important to collect every photon and preserve uniform sensitivity across the pixel area.

PHOTON-COUNTING DETECTOR DESIGN

The GM-APD (see Figure 3) used in this project is a separate-absorber-and-multiplier (SAM) structure fabricated in a lightly p-doped (10^{14} boron atoms/cm^3) epitaxial layer grown on top of a heavily p-doped (10^{18} boron atoms/cm^3) silicon substrate. The diode is fabricated by ion implantation of n-type (arsenic and phosphorus) and p-type (boron) dopants to form, from the surface down, an (n+)–π–(p+)–π–(p+ substrate) structure (π denotes very lightly p-doped) on a silicon substrate. The substrate is removed by backside thinning and is passivated with a thin p+ layer. When reversed biased, there is a modest electric field (10^4 V/cm) established in the first π layer (absorber) forcing photoelectrons to drift into the second π layer (multiplier). The field in the multiplier layer is stronger (several 10^5 V/cm), sufficient to cause impact ionization that initiates the avalanche discharge. The photoelectron and the secondary electrons are collected at the n layer, and the photo-hole and secondary holes are collected at the substrate side. The n+ implant extends beyond the multiplier region, forming a guard ring that collects dark current generated between pixels. This dark current does not initiate avalanche discharges, and so will not cause detection events. Extending the n+ implant beyond the p layer also prevents breakdown at the periphery of the GM-APD, since the electric fields are much lower than in the multiplier region.

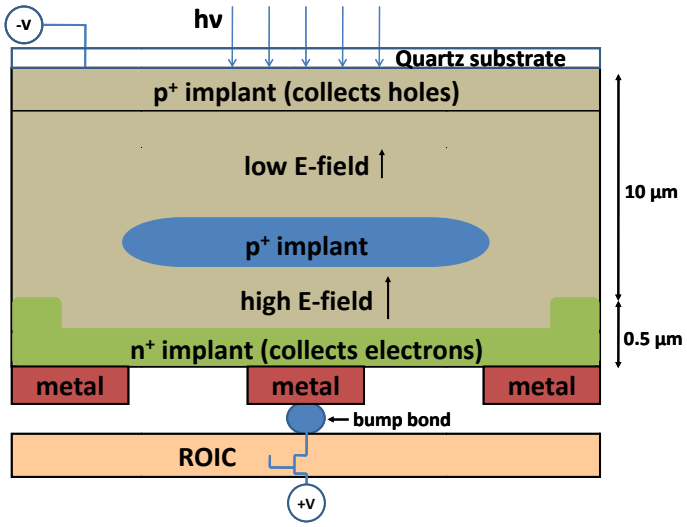

Figure 3. This diagram shows a schematic cross-section of a GM-APD. It shows the low field region where photons are converted into electron-hole pairs and the high field region where electrons are accelerated.

Figure 4 shows a cross-section of two versions of the APD, one using a low-fill-factor design and the other using a high-fill-factor design. Both designs are intended to be used in a backside illuminated configuration. On the right of the figure, the shallow portion of the stepped p+ implant separates the absorber and multiplier portions of each detector. The step lowers the electric field at the edges of the diode, preventing edge breakdown and forming a guard ring to collect surface-generated dark current without multiplying it. The deep portion of the implant, which is partially undepleted, prevents the guard ring from collecting photoelectrons generated in the absorber; these photoelectrons reach a nearby multiplier region by a combination of diffusion and drift.

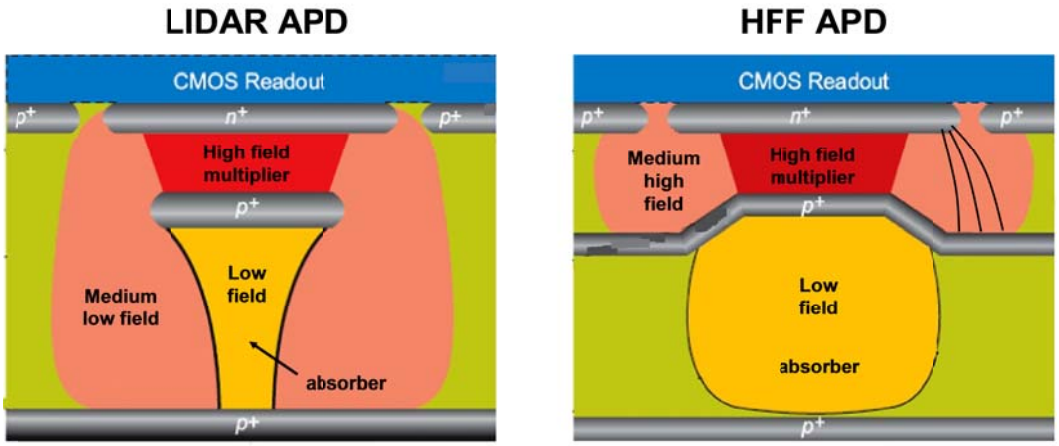

Figure 4. Cross-sections of two APD designs, one using a low-fill-factor design suitable for LIDAR (left) and the other using a high-fill-factor design suitable for imaging applications (right). Photons are absorbed in the "absorber" regions. Charge is multiplied in the "multiplier" regions.

A 256×256 CMOS ROIC (see Figure 5) has been designed and fabricated with 25-µm pixels, based on an innovative approach to managing the tradeoff between pixel real estate and readout bandwidth. Each pixel has a flip-flop that is set whenever a photon detection has occurred. In addition, there is a modest-sized (7-bit) pseudorandom counter that counts

detection events. When the 7-bit counter overflows, it sets an overflow flip-flop and continues counting from zero. The chip has two independent readout systems, one for reading out the detection flip-flops and another for reading out the counter overflow flip-flops. Each system addresses successive rows or columns of pixels, reading out and clearing the flip-flops, while the pixels continue to stare and register events. For low fluxes, individual detection events can be recorded. At higher fluxes, the overflow bits can be recorded; each represents the detection of 127 photons. There is also a mechanism to readout the entire contents of the 7-bit counters.

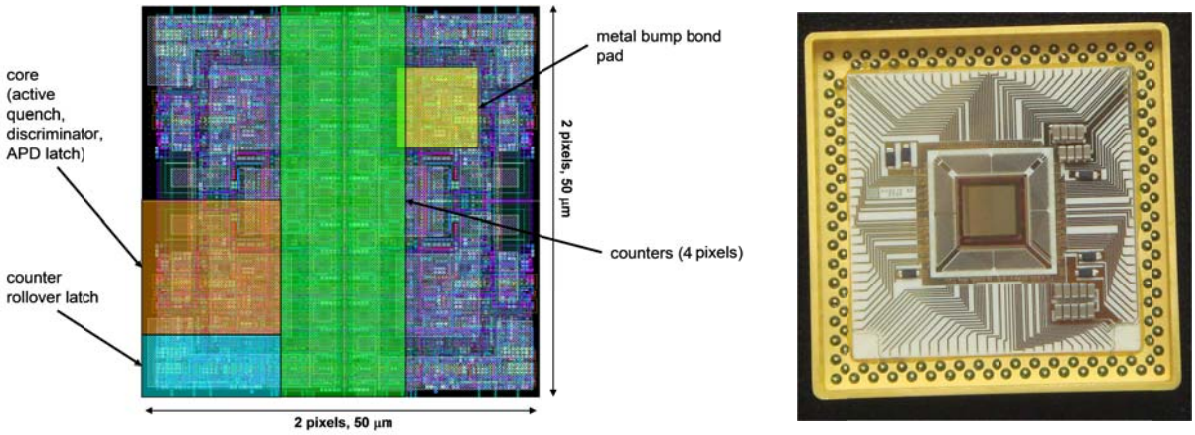

Figure 5. (left) Floorplan of the unit cell (2×2 pixels) for a previously-designed 256×256 pixel CMOS ROIC. (right) Photograph of this ROIC.

PROTOTYPE DEVICE CHARACTERISTICS

A working prototype of a 256×256 low-fill-factor APD hybridized to a CMOS ROIC has been fabricated and tested. The clock patterns for the APD are shown in Figure 6. In Geiger mode, the APD is biased above the breakdown voltage before the APD can detect a photon. This "arming" of the APD takes place over the duration of the arm pulse ("a" in Figure 6). Once an avalanche takes place, the APD must be refreshed and "re-armed" in order to be able to detect photons again. This can be done in the single gate mode, in which each "re-arm" takes place when desired in a single shot, or the continuous gate mode in which the "re-arm" occurs at a regular interval, τ, as in Figure 6. The APD is ready to detect a photon over the gate width of τ–a. If a photon arrives during that time, it initiates an avalanche and the flip flop on the ROIC registers an event. Other photons arriving during that time do not register an event, as the APD is already avalanching. Then, for a flux, ρ, on the APD, the trigger probability per gate is the Poisson probability of one or more photons arriving over τ, which is just $1–\exp^{-\rho\tau}$.

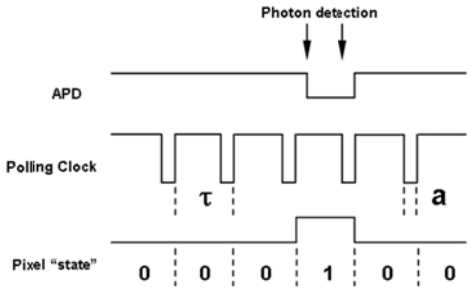

Figure 6. Clock patterns for the APD. This picture holds for both photons and dark events.

The exponential nature of the triggering probability can be seen in Figure 7 (*left*). A series of dark current exposures lasting 50,000 gates were taken in the single gate mode with a = 100 ns and τ = 0.5–4000 μsec. The experimental event trigger probability, calculated by dividing the number of triggered gates by the total number of gates, closely follows the

expected triggered probability of $1–\exp^{-\rho\tau}$. The event trigger probability grows linearly with the gate width for very small gate widths, and it begins to "saturate," asymptotically reaching 1 as the gate width increases even further. The dark count rate for the pixels, calculated by fitting the data to $1–\exp^{-\rho\tau}$, are between 0.1 to 10 kHz per pixel.

The data used to plot Figure 7 (*left*) were obtained by reading out the flip-flop that records a single event at each pixel. While this mode has the advantage of being able to time stamp each event, it is also only suitable for a low flux as reading out every pixel is an expensive operation and is the bottleneck in the whole exposure sequence. This necessitates a long τ or long dead time between two adjacent gates. For high flux, the periphery data mode is the more appropriate readout choice. While the possibility of having a time stamp for each event is lost, reading out only the overflow counter in the 7-bit counters in each pixel allows for a 100 times slower readout rate than otherwise. Hence, the APD can be operated with short gates, greatly reducing dead time.

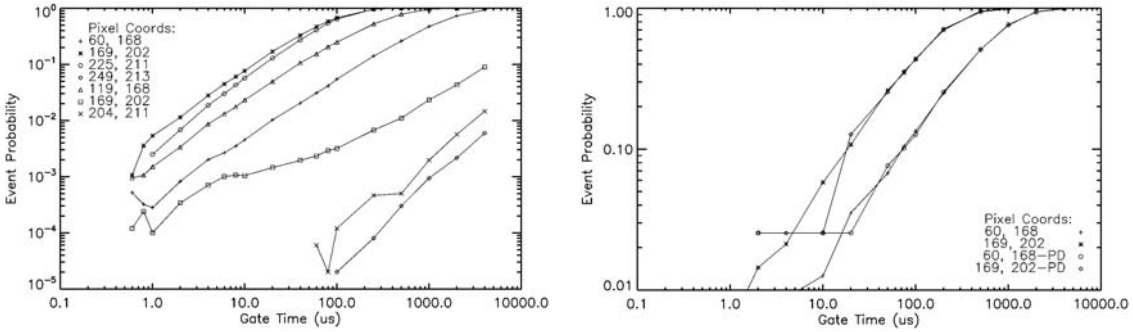

Figure 7. (*left*) Event trigger probability for pixels on the APD with T=185 K, a = 100 ns, τ = 0.5 to 4000 μsec. Event probability is the number of triggered gates divided by the total number of gates. (*right*) Event trigger probability for pixels at 185 K. The points labeled with 'PD' are data obtained by reading out the overflow counter in the periphery data mode. The event trigger probabilities obtained with the flip-flop data are also shown for comparison.

The event trigger probabilities for pixels calculated using the overflow counter data in the periphery data mode for 5,000 gates are shown in Figure 7 (*right*). As expected the event trigger probabilities match very well those calculated with the flip-flop data. The discrepancies for the shortest gate widths are caused by the small number of triggered events and the coarse nature of the overflow data, where it is only in increments of 127 events. This will be remedied by reading out the remaining 7-bit counter values at the end of the exposure. The periphery data mode will be essential for applications where a high photon flux is likely.

Figure 8 shows an image created by placing an Air Force target on top of the detector and illuminating it with a light source. The image was taken with the detector at room temperature and exposed to ambient light levels. It is the sum of 1000 gate exposure sequences in which only one photon is counted per gate. The event flip-flop for each pixel is read out after each gate and saved for later processing. The events generated by dark current are mitigated by setting a small gate time in which the APDs are above breakdown and able to achieve a GM avalanche.

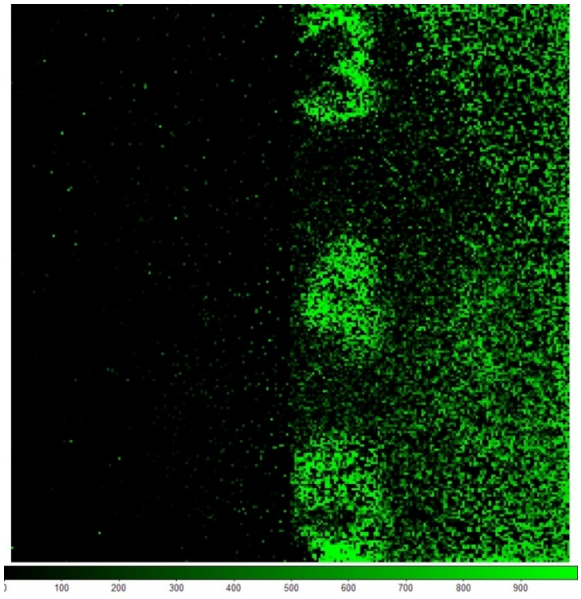

Figure 8. This is an image taken with a GM-APD array biased above breakdown.

Figure 9 shows how the IV characteristic of the GM APDs changes with temperature. The breakdown voltage is estimated from this type of plot as the point on this surface plot where the anode current sharply increases.

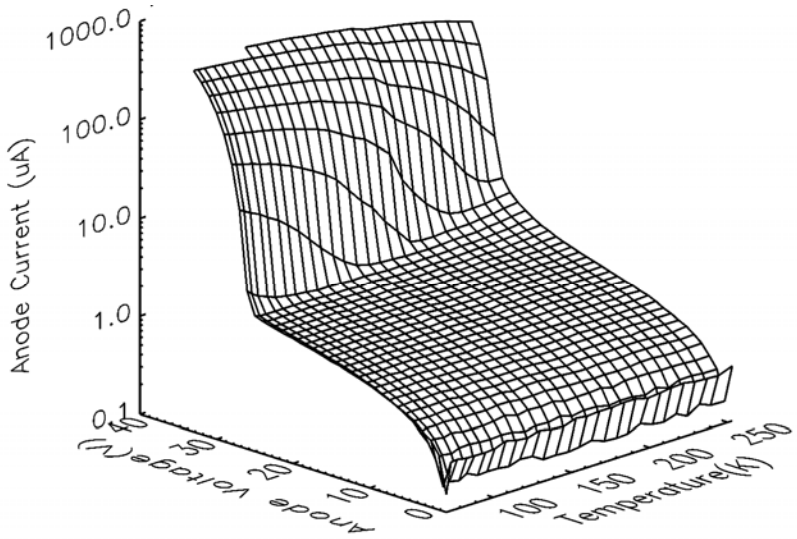

Figure 9. This is a plot of the anode current vs. anode voltage and temperature.

ACKNOWLEDGEMENTS

This project was funded by the Gordon and Betty Moore Foundation.

REFERENCES

[1] J. T. Trauger and W. A. Traub, "A laboratory demonstration of the capability to image an Earth-like extrasolar planet," *Nature*, vol. 446, p. 771, 2007.

[2] "TPF-C Flight Baseline Mission Concept Report,". [Online]. http://planetquest.jpl.nasa.gov/TPF-C/TPFC-MissionAstro2010RFI-Final-2009-04-01.pdf

[3] "TPF-C STDT Report,". [Online]. http://planetquest.jpl.nasa.gov/TPF/STDT_Report_Final_Ex2FF86A.pdf

[4] D. F. Figer et al., "Independent Testing of JWST Detector Prototypes," *SPIE*, vol. 5167, p. 270, 2004.

[5] F Gillett, "Near IR WFSing For Gemini," Gemini Observatory, Tucson, Internal Report 1995.

[6] O. Daigle et al., "Extreme Faint Flux Imaging with an EMCCD," *PASP*, vol. 121, p. 866, 2009.

[7] P. J. Pool et al., "Application of electron multiplying CCD technology in space instrumentation," *SPIE*, vol. 5902, p. 67, 2005.

[8] O. Daigle et al., "CCCP: a CCD controller for counting photons," *SPIE*, vol. 7014, pp. 70146L-70146L-10, 2008.

[9] B. J. Hadwen, M. A. Camas, and M. S. Robbins, "The Effects of Co ^60 Gamma Radiation on Electron Multiplying Charge-Coupled Devices," *IEEE Transactions on Nuclear Science*, vol. 51, no. 5, pp. 2747-2752, 2004.

[10] David R. Smith, Richard Ingley, and Andrew D. Holland, "Proton Irradiation of EMCCDs," IEEE Transactions on Electron Devices," vol. 53, no. 2, 2006.

[11] Robert F. Pierret, *Semiconductor Device Fundamentals*. Reading, Mass: Addison-Wesley Publishing Company, 1996.

[12] S. Cova, M. Ghioni, A. Lacaita, and F. Zappa, "Avalanche photodiodes and quenching circuits for single-photon detection," *Applied Optics*, vol. 35, pp. 1956-1976, 1996.

[13] M. A. Albota et al., "Three-dimensional imaging laser radar with a photon-counting avalanche photodiode array and microchip laser," *Appl Opt.*, vol. 41, no. 36, pp. 7671-8, Dec 2002.

[14] B. F. Aull, "3D Imaging with Geiger-mode Avalanche Photodiodes," *Optics and Photonics News* , vol. 16, pp. 42-46, 2005.

[15] B. Aull et al., "Laser radar imager based on three-dimensional integration of Geiger-mode avalanche photodiodes with two SOI timing-circuit layers," *ISSCC Dig. Tech. Papers*, pp. 304-305, 2006.

[16] R. M. Marino et al., "A compact 3D imaging laser radar system using Geiger-mode APD arrays: system and measurements," *SPIE*, vol. 5086, pp. 1-15, 2003.

[17] N. J. Woolf, P. S. Smith, W. A. Traub, and K. W. Jucks, "The Spectrum of Earthshine: A Pale Blue Dot Observed from the Ground," *ApJ*, vol. 574, p. 43, 2002.